IEEE Access
Multidisciplinary | Rapid Review | Open Access Journal

Received September 30, 2019, accepted October 24, 2019, date of publication November 11, 2019,
date of current version November 21, 2019.

Digital Object Identifier 10.1109/ACCESS.2019.2952933

A 20-GHz-Band 64 × 64 Hollow Waveguide Two-Dimensional Butler Matrix

TAKASHI TOMURA[1], (Member, IEEE), DONG-HUN KIM[1], (Graduate Student Member, IEEE), MASAHIRO WAKASA[1], YUKI SUNAGUCHI[1], JIRO HIROKAWA[1], (Fellow, IEEE), AND KENTARO NISHIMORI[2], (Member, IEEE)

[1]Department of Electrical and Electronic Engineering, Tokyo Institute of Technology, Tokyo 152-8552, Japan
[2]Graduate School of Science and Technology, Niigata University, Niigata 950-2181, Japan

Corresponding author: Takashi Tomura (tomura@ee.e.titech.ac.jp)

This work was supported in part by the Strategic Information and Communications Research and Development Promotion Programme (SCOPE), in part by the Ministry of Internal Affairs and Communications under Grant 165004002 and Grant 185004002, and in part by KAKENHI Aid for Scientific Research (B) under Grant 17H03262.

ABSTRACT In this paper, a 20-GHz-band 64 × 64 hollow waveguide Butler matrix is proposed. By using two-plane short slot couplers and a modified diagram, a short-axis two dimensional Butler matrix is realized. The design method of the diagram and components is presented. The Butler matrix is composed of two plane hybrids, cross couplers and phase shifters. The designed Butler matrix is fabricated by milling and screwing together nine aluminum plates. The dimensions and weight are 86.40 mm × 74.19 mm × 396.34 mm and 7.0 kg, respectively. Transmission characteristics as a beam switching circuit are characterized by measurements, with a low insertion loss of less than 1.8 dB and an excitation error of 4-dB and 40-deg. standard deviation. Radiation characteristics as a 64-beam antenna are measured, and a wide coverage area of 40% of the hemisphere and high directivity of more than 18.7 dBi were determined by measurements.

INDEX TERMS Butler matrix, hollow waveguide, two dimensional beam switching, two-plane short slot coupler.

I. INTRODUCTION

Beam steering/switching/forming is one of the key technologies to realize advanced mobile wireless communication. Moreover, massive multi-beam circuits are also essential to enable massive MIMO systems which are one of main technologies in Fifth Generation (5G) systems [1]. In 3GPP Release 15 [2], [3], it is prescribed to use hybrid beamforming [4] which includes analog beamforming networks called radio distribution networks (RDN). To achieve this, Butler matrices [5] have been widely researched as a beam-forming network. These have unique features such as theoretically lossless, spatially orthogonal beams, and offer scalability in the number of beams. A large number of beams, high gain, and wide coverage area are required in antennas for base stations.

There are many reports on improving beam forming networks and extending their function. In [6], a dual polarized Butler matrix has been proposed by square waveguides and dual polarized hybrids and cross overs. The number of beams by Butler matrices is limited to 2^N. In [7], a 9 × 9 beam forming network has been proposed by three-way couplers at 28 GHz. New configurations have been proposed for beam direction control by an asymmetric configuration of phase shifters [8] or reconfigurable couplers [9].

Several kinds of transmission lines or waveguides have been used for the Butler matrices such as waveguides [10], microstrip lines [11], [12], strip lines [13], and substrate integrated waveguides (SIW) [14]. The transmission loss of these transmission lines is 0.04 dB/cm at 90 GHz [15], 0.22 dB/cm at 24 GHz [16], 0.115 dB/cm at 26.25 GHz [17], and 0.15 dB/cm at 26 GHz [18], respectively. Among the transmission lines, hollow waveguides are superior candidates to realize low insertion loss and high efficiency in the millimeter wave band. Transmission lines using dielectric materials have higher losses in the millimeter wave band.

The 2D beam switching can be created by cascading 1D beam switching circuits [19]–[23]. The number of beams are expanded to 4 × 4 in these papers. The length of the Butler matrix increases as the number of beams increase, making it desirable that each component of the Butler matrices should be as short as possible. Much research has investigated how

The associate editor coordinating the review of this manuscript and approving it for publication was Sudipta Chattopadhyay.

to reduce the length of each component [11], [14], [24]–[28]. In [26], a cruciform directional coupler has been designed to reduce the length. The shape of the coupling region has been optimized for wideband characteristics [27] and arbitrary power ratios [28]. However, the length of the 2D Butler matrices are basically limited by the diagram cascading 1D Butler matrices.

Another method to reduce the length of the 2D Bulter matrices is to use two-plane couplers. Two-plane couplers have been proposed to reduce the length to half [29]. Because of the two-plane coupler components, the diagram can be simplified and the number of cascaded components becomes half of that of the conventional 2D Butler matrix composed of cascaded 1D Butler matrices. Using two-plane couplers, a 16 × 16 2D Butler matrix has been proposed and fabricated [30]. However, the number of beams, directivity, and coverage are limited to 4 × 4, 11.8 dBi −18.7 dBi and 31% of the hemisphere, respectively. A larger number of beams, higher directivity, and wider coverage are required for advanced base stations.

We have proposed a 64 × 64 2D Butler matrix [31], [32] to increase the number of beams to 8 × 8, directivity, and coverage area. However, the method of configuration and the effectiveness of the 64 × 64 2D Bulter matrix has not been shown in detail.

This paper details the configuration method of the 64 × 64 2D Butler matrix using two-plane couplers, and this method can be scaled to any $2^n \times 2^n$ 2D Butler matrix. Here, a 64 × 64 2D Butler matrix for the 20-GHz-band is designed and fabricated. The fabricated Butler matrix is characterized by measuring the transmission characteristics such as the transmission amplitude and phase, insertion loss and reflection. The radiation characteristics as a 64-beam antenna is also evaluated by a planar and cylindrical near-field antenna measurement system. Radiation patterns and coverage area are also characterized.

II. TWO-DIMENSIONAL BUTLER MATRIX CONFIGURATION METHOD

The configuration method for the short-axis two-dimensional 64 × 64 Butler matrix is described in this chapter. The method consists of 4 steps as follows:

Step 1. Prepare a one-dimensional 8 × 8 Butler matrix. The number of ports (8) are the square root of the two-dimensional matrix (64). In this paper, the diagram shown in Fig. 1 is used and it is composed of hybrids, cross couplers, and phase shifters.

Step 2. Cascade vertically and horizontally into eight stacked Butler matrices as suggested in Fig. 2. This diagram is the same as for conventional two-dimensional Butler matrices [20]–[23].

Step 3. Rearrange the components so the same type of components are continuously cascaded as in Fig. 3. This is based on the idea that horizontally and vertically stacked components are interchangeable [30].

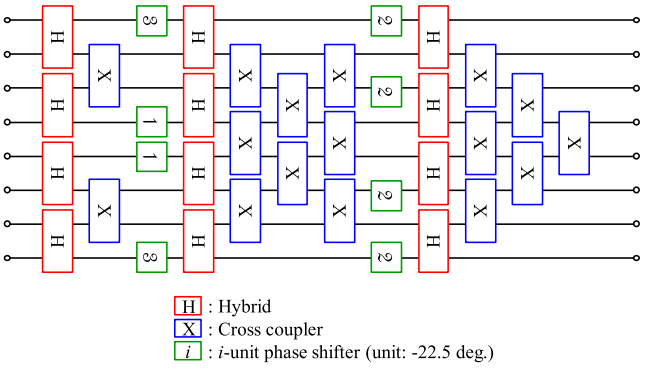

FIGURE 1. 8 × 8-way Butler matrix diagram.

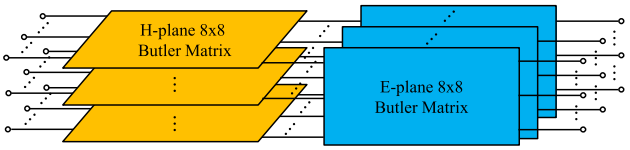

FIGURE 2. Conventional 64 × 64-way Butler matrix.

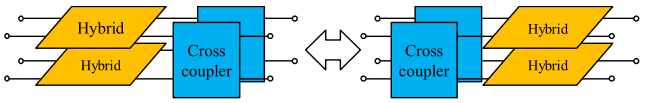

FIGURE 3. Interchange of horizontally and vertically stacked components.

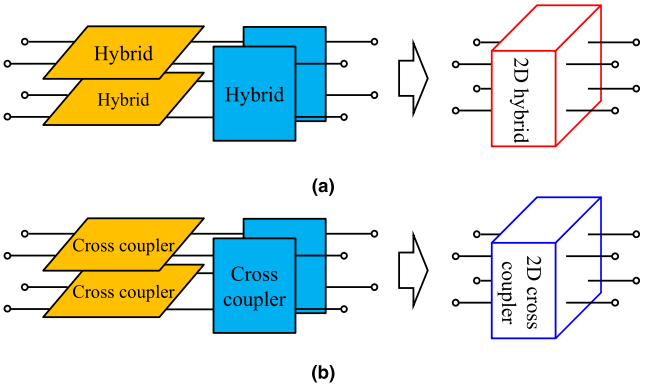

FIGURE 4. Two combined horizontally and vertically cascaded stacked components of (a) hybrid and (b) cross couplers.

Step 4. Combine two continuously cascaded hybrids and cross couplers into two-dimensional hybrid or cross couplers as shown in Fig 4. Combine two continuously cascaded phase shifters into one phase shifter with summed phase shift values.

The result is the diagram of a two dimensional 64 × 64 Butler matrix as shown in Fig. 5. The components in each of the units are shown in Figs. 6 to 8. They are configured by combining components horizontally and vertically as detailed in step 4. The difference between the diagrams of the 8 × 8 1D (Fig. 1) and 64 × 64 2D (Fig. 5) Butler matrices is that all components become 2D ones with summed phase shift values. Compared with the conventional 64 × 64 Butler matrix (Fig. 2), the proposed 64 × 64 2D Butler matrix has half the number of cascaded components. This is the reason

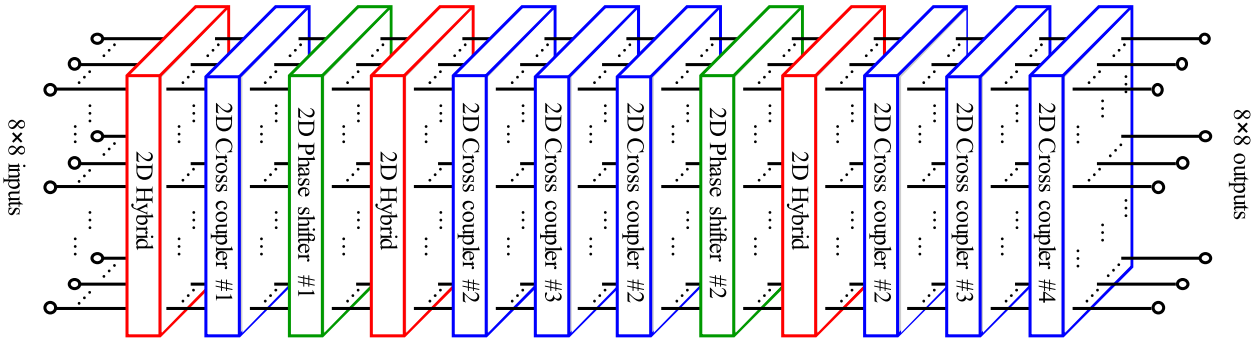

FIGURE 5. 64 × 64 2D Butler matrix.

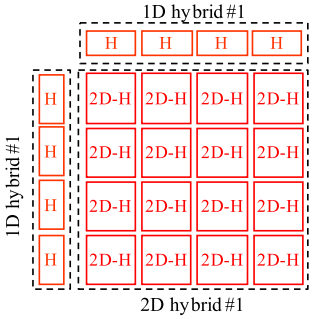

FIGURE 6. 2D hybrid.

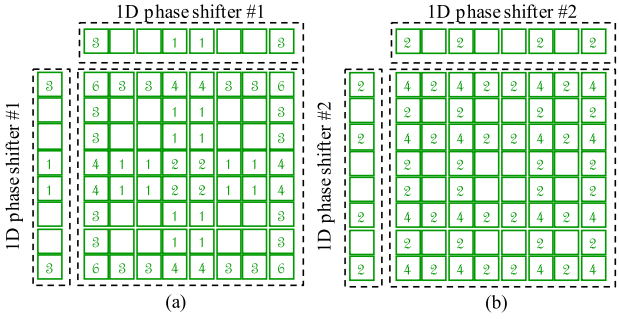

FIGURE 8. 2D phase shifters (a) #1, (b) #2.

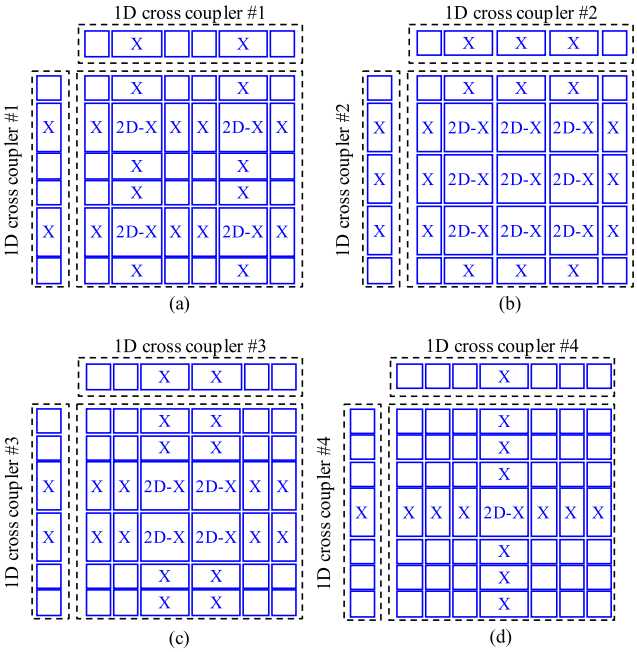

FIGURE 7. 2D cross couplers (a) #1, (b) #2, (c) #3, (d) #4.

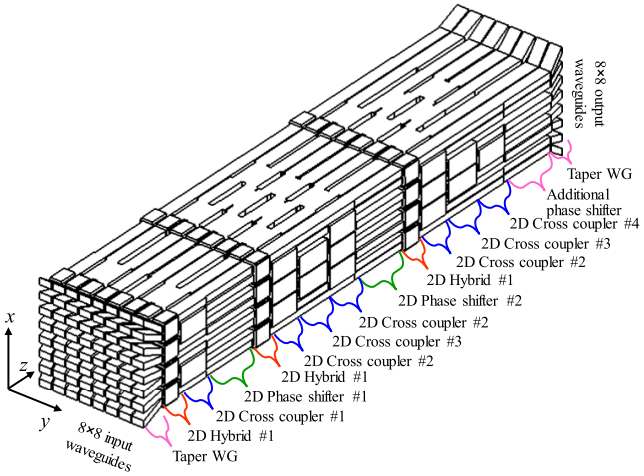

FIGURE 9. The 64 × 64 2D waveguide Butler matrix.

why the 2D Butler matrix using two-dimensional components enables shorter axis lengths.

III. DESIGN OF THE 64 × 64 2D BUTLER MATRIX BY WAVEGUIDES

The 64 × 64 2D Butler matrix detailed in the previous chapter is designed by waveguides. The design frequency is 19.55 GHz. All components, hybrids, cross couplers, and phase sifters are designed based on [29] and [30].

The designed 64 × 64 Butler matrix is shown in Fig. 9. Because the transmission phases of the cross couplers are different for the 1D and 2D components, additional phase sifters are added after the 2D cross coupler #4. The details of the additional phase shifters are shown in Appendix A. Taper waveguides are added in the input and output ports to make the element spacing 9.9 mm (0.65 free space wavelength).

The transmission characteristics as well as the radiation characteristics are simulated by the finite element method. The definition of the input and output ports is shown in Fig. 10. The structure is symmetric with respect to the two

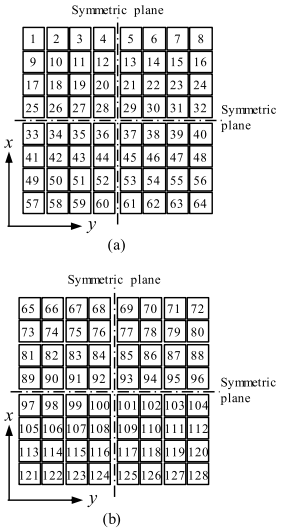

FIGURE 10. Port numbering. (a) Input ports. (b) Output ports.

TABLE 1. Symmetric ports.

Input ports				Output ports			
1	8	57	64	65	72	121	128
2	7	58	63	66	71	122	127
3	6	59	62	67	70	123	126
4	5	60	61	68	69	124	125
9	16	49	56	73	80	113	120
10	15	50	55	74	79	114	119
11	14	51	54	75	78	115	118
12	13	52	53	76	77	116	117
17	24	41	48	81	88	105	112
18	23	42	47	82	87	106	111
19	22	43	46	83	86	107	110
20	21	44	45	84	85	108	109
25	32	33	40	89	96	97	104
26	31	34	39	90	95	98	103
27	30	35	38	91	94	99	102
28	29	36	37	92	93	100	101

symmetric planes indicated in Fig. 10. The symmetric ports are listed in Table 1.

The transmission characteristics are shown in Fig. 11. Standard deviations of the transmission amplitude are calculated using dB values and is less than 3.1 dB at the design frequency. The standard deviation of the difference between the transmission phase and the ideal is less than 19.6 deg. at this design frequency.

The frequency characteristics of the reflections of port 1 are shown in Fig. 12. The reflection is less than −18.5 dB at the design frequency and less than −10 dB from 19.3 GHz to 20.0 GHz.

A low insertion loss < 1.6 dB at the central frequency is realized as shown in Fig. 13. The insertion loss of the input port n IL_n is calculated as follows.

$$IL_n = \sum_{m=65}^{128} \left|S_{m,n}\right|^{-2} \tag{1}$$

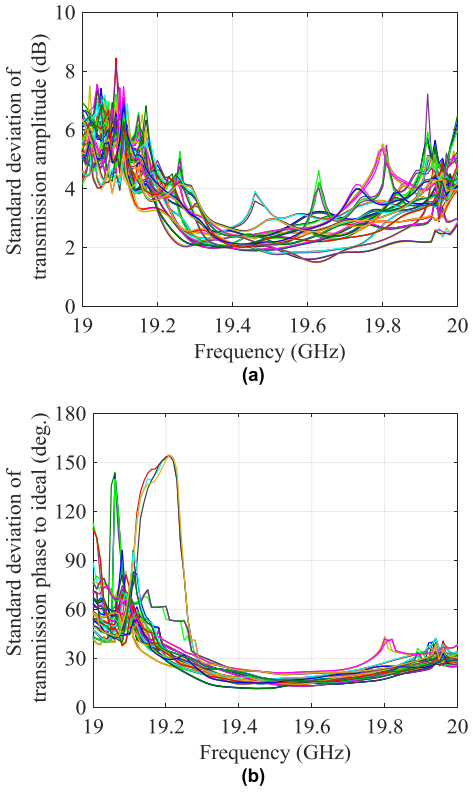

FIGURE 11. Standard deviation of transmission characteristics of (a) amplitude, (b) differences between transmission phase and the ideal.

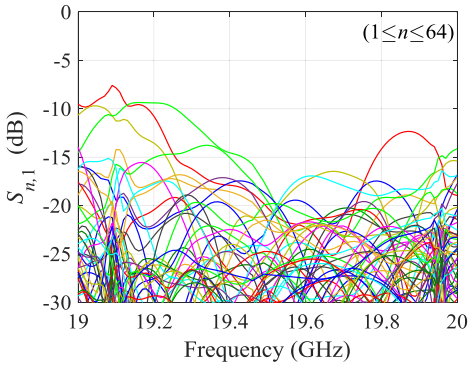

FIGURE 12. Frequency characteristics of the reflection (input port: 1).

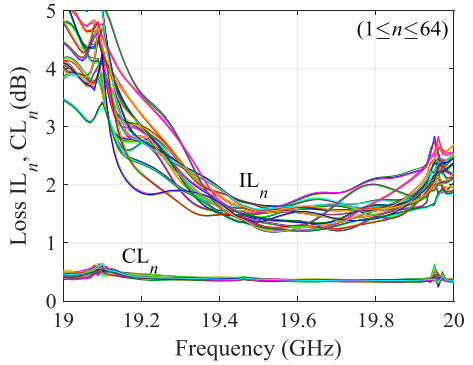

FIGURE 13. Frequency characteristics of insertion and conductor losses.

The conductor loss of input port n CL_n is less than 0.4 dB at the design frequency as also shown in Fig. 13. The conductor

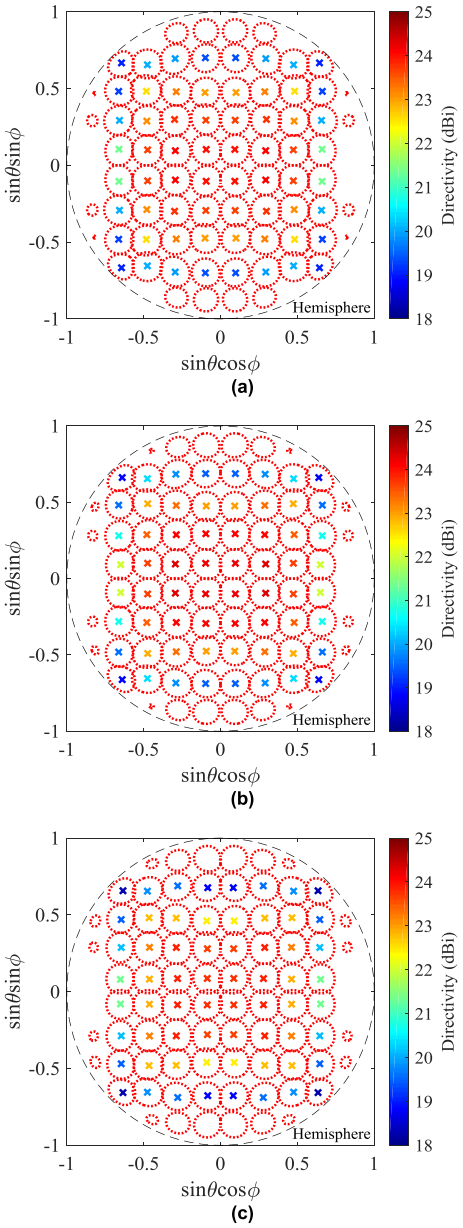

FIGURE 14. Peak direction and 3.9-dB contour of radiation patterns at (a) 19.39 GHz, (b) 19.55 GHz, and (c) 19.75 GHz.

loss is calculated from the difference in the insertion loss between aluminum and PEC models. The remaining part of the insertion loss results from the return loss.

The beam peak direction, directivity, and 3.9-dB contour of the radiation patterns are shown in Fig. 14. The beam peak directions align in a lattice pattern. The directivity is from 18.8 dBi to 24.2 dBi. The total coverage, which is defined by the 3.9-dB contour of the main beam, is 2.55, 2.46, and 2.45 steradians at 19.39, 19.55, and 19.75 GHz, respectively, which corresponds to 40.6%, 40.2%, and 39.0% of the hemisphere.

The frequency characteristics of the realized gain is shown in Fig. 15, showing a 1-dB down gain bandwidth of more than 2.5%. The peak realized gain is different at different input

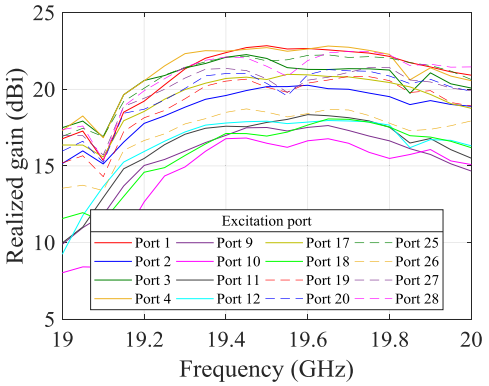

FIGURE 15. Frequency characteristics of the realized gain.

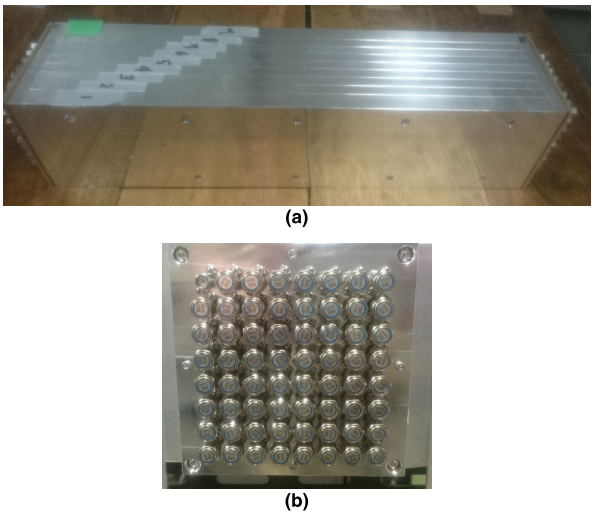

FIGURE 16. Fabricated 64 × 64 Butler matrix. (a) Assembled 64 × 64 waveguide Butler matrix. (b) Input / output ports with loads.

ports because the beam direction is different and as the scan loss is affected by the beam direction.

IV. MEASURED RESULTS

The designed 64 × 64 waveguide Butler matrix was fabricated by milling nine aluminum (A6061) plates and screwing them together. The assembly is shown in Fig. 16, and the dimensions and weight are 86.40 mm × 74.19 mm × 396.34 mm and 7.0 kg, respectively. Coaxial (SMA)-waveguide transitions are connected for the measurements. Transmission and radiation characteristics were evaluated by the measurements.

A. TRANSMISSION CHARACTERISTICS

The transmission characteristics were measured by a two-port vector network analyzer. Specifically, S_{mn}, $m \in \{1, 2, 9, 10\}$, $n \in \{65, 66, \ldots, 128\}$, were measured to evaluate reflection, transmission, and insertion loss. During the measurements the non-measured ports were terminated by load terminations.

The frequency characteristics of the reflection are shown in Fig. 17. The reflections are well suppressed, below −10 dB from 19.2 GHz to 19.8 GHz.

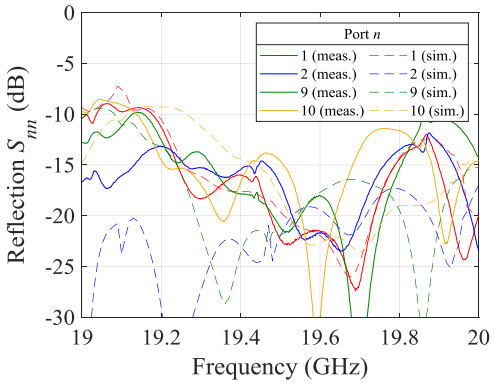

FIGURE 17. Frequency characteristics of the reflections.

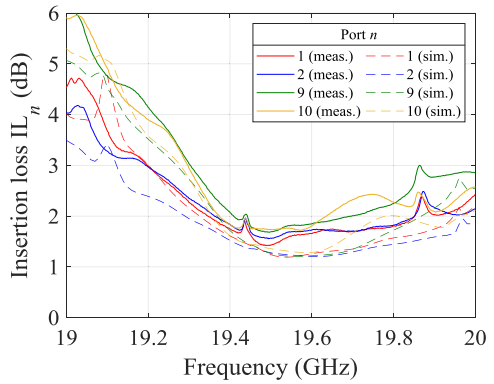

FIGURE 18. Frequency characteristics of the insertion losses.

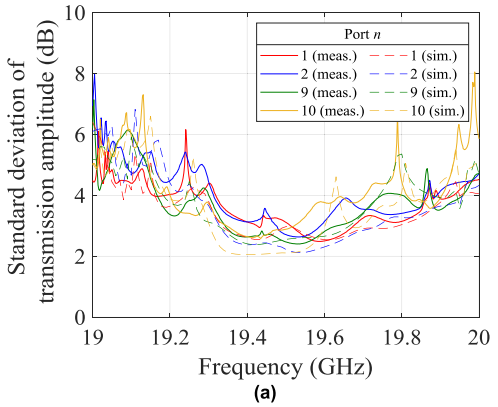

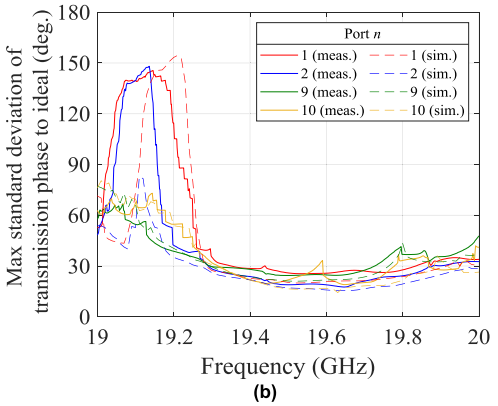

FIGURE 19. Standard deviations of transmission characteristics. (a) Amplitude. (b) Difference between the transmission phase and the ideal.

The frequency characteristics of the insertion loss are shown in Fig. 18. A low insertion loss is also verified by the measurements. The highest measured insertion loss at the design frequency is 1.8 dB, 0.6 dB higher than the simulated value.

Standard deviations of the transmission characteristics are shown in Fig. 19, here the measured values agree with the simulations. The amplitude standard deviation is less than 4 dB from 19.3 GHz to 19.7 GHz. The phase standard deviation is less than 40 deg. from 19.3 GHz to 19.8 GHz.

B. RADIATION CHARACTERISTICS

Radiation characteristics were measured by near-field antenna measurements (NFAM), and a quarter of the antenna ports were measured considering the symmetricity of the structure. A planar NFAM was used as shown in Fig. 20, the scan area and step length are 1136 × 1136 mm^2 and 7.1 mm, respectively. A cylindrical NFAM system was also used for 4 ports, ports 10, 11, 12, and 18, because of their wide beam scan angle. Here the scanned area is 2100 mm in the vertical direction and ±180 degree in the azimuth direction with 7.5-mm and 1-degree steps.

The peak directivity directions and 3.9-dB-directivity-down contours at 19.39, 19.55, and 19.75 GHz are shown in Fig. 21. The measured results agree with the simulations. The maximum difference in the beam direction between the simulations and the measurements is 2.5 deg. for port #12 at

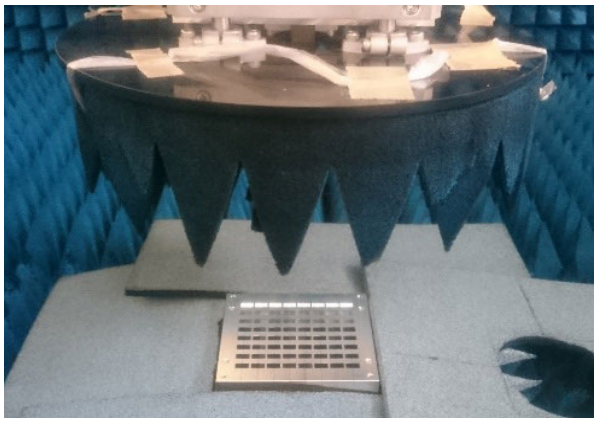

FIGURE 20. Measurement arrangements of radiation characteristics by planar near-field antenna measurement.

the design frequency. The measured total areas of coverage, which are defined by the 3.9-dB contour of the main beam, are 0.65, 0.64, and 0.63 steradians at 19.39, 19.55, and 19.75 GHz, respectively, which correspond to 41.0%, 40.5%, and 40.4% of the quarter hemisphere.

The measured radiation patterns in the E-plane are plotted in Fig. 22 with the simulated patterns, showing that they agree well. The peak directivity is listed in Table 2. Only a quarter of the ports were measured considering the symmetricity of the structure, and it may be expected that the symmetric ports

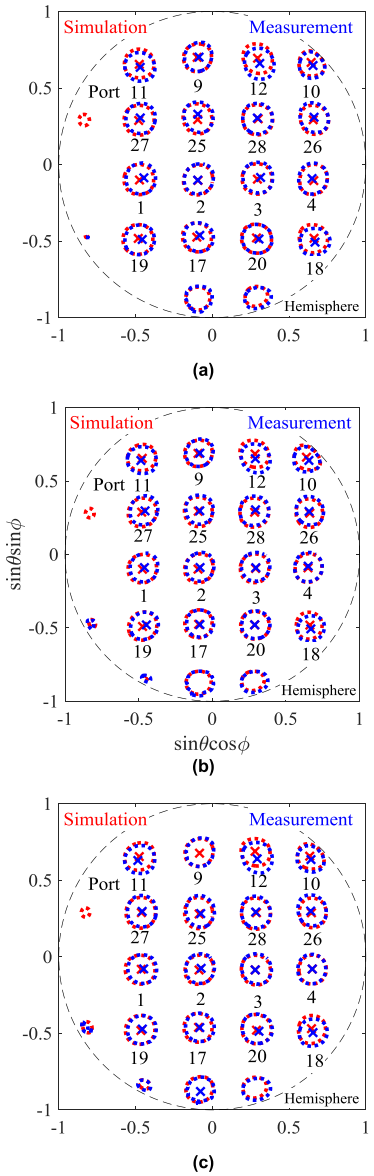

FIGURE 21. Peak directivity directions and 3.9-dB-directivity-down contours at (a) 19.39 GHz, (b) 19.55 GHz, (c) 19.75 GHz.

TABLE 2. Peak directivity at the design frequency.

Port	Simulated (dBi)	Measured (dBi)	Difference (dB)
1	24.2	23.9	0.3
2	22.0	20.7	1.3
3	23.6	23.0	0.6
4	24.2	24.0	0.3
9	19.4	18.7	0.7
10	18.8	18.7	0.1
11	20.3	19.6	0.7
12	19.8	19.0	0.9
17	23.0	23.1	-0.1
18	19.5	19.1	0.4
19	22.9	23.0	-0.2
20	23.3	23.1	0.1
25	24.0	24.1	0.0
26	20.7	19.6	1.1
27	23.4	22.9	0.5
28	24.0	23.7	0.4

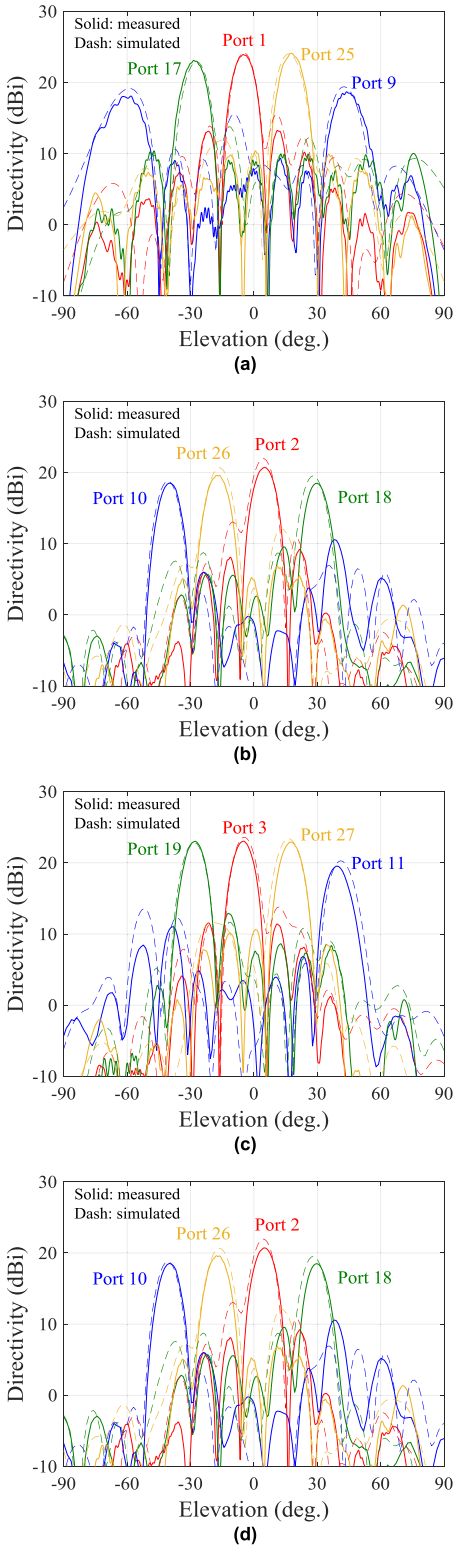

FIGURE 22. E-plane radiation patterns at the design frequency. (a) Input ports 1, 9, 17, 25, (b) 2, 10, 18, 26, (c) 3, 11, 19, 27, (d) 4, 12, 20, 28.

indicated in Table 1 have the same level of directivity. The maximum directivity decrement compared with the simulations is 1.3 dB.

TABLE 3. Details of the proposed and reported beam forming network particulars.

Ref.	Number of beams	Trans-mission Line	Frequency (GHz)	Gain (dBi)	Coverage of hemisphere (%)
[20]	4×4	SIW	29	4.4 - 6.8	NA
[21]	4×4	SIW	60	10 - 14.7	NA
[22]	4×4	SIW	30	10.6 - 15.9	NA
[23]	4×4	MSL	60	6.5 - 8.4	NA
[30]	4×4	Waveguide	22	11.8 - 18.7	31
This work	8×8	Waveguide	19.55	16.9 - 22.3	40

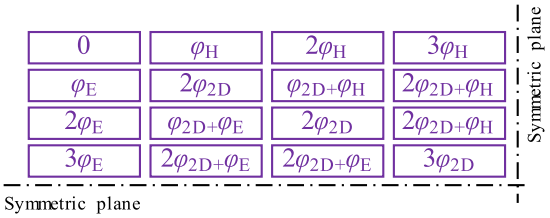

FIGURE 23. Phase shift amounts of the additional phase shifter.

Details of the particulars of the beam forming networks are shown in Table 3. The proposed network realizes the maximum number of beams as well as the highest gain. The coverage of the hemisphere is 40%, 9% higher than that of [30].

V. CONCLUSION

In this paper, a 20-GHz-band 64 × 64 Butler matrix is proposed. Composition of the diagram using two-plane couplers and its design results are described. The designed Butler matrix was fabricated by milling and screwing together aluminum plates. The transmission characteristics as a beam switching circuit and the radiation characteristics as a 64-beam switching antenna are characterized. Low insertion losses and low excitation errors are determined as well as a wide coverage area and high directivity. The proposed Butler matrix would be an attractive candidate as antennas in base stations for future wireless communication system. Other fabrication methods such as additive manufacturing or diecasting may reduce the cost of the Butler matrix.

APPENDIX A
PHASE COMPENSATION OF CROSS COUPLERS

The transmission phase of each of the cross couplers is different and is required to be compensated for. The transmission phase relative to a straight waveguide is defined as $-\varphi_{2D}$, $-\varphi_E$, and $-\varphi_H$ for the 2-d, E-, and H-plane cross couplers, respectively. The phase shift amounts are shown in Fig. 23. The phase shift amount is determined by the number and the type of cross couplers that are passed. For example, the power arriving at the southeast port passes the E-plane cross coupler twice and the 2d coupler once, giving a phase shift amount of $2\varphi_E + \varphi_{2D}$. In this study, the designed cross couplers have transmission phases of $-\varphi_{2D} = 86.6$ deg., $-\varphi_E = -96.3$ deg., and $-\varphi_H = 29.6$ deg at the design frequency.

ACKNOWLEDGMENT

The authors wish to thank Drs. S. Kurokawa, M. Ameya, and Y. She for their support in the cylindrical near-field antenna measurements.

REFERENCES

[1] K. Nishimori, "Novel technologies using massive MIMO transmission toward 5G and its beyond systems," in *Proc. Int. Symp. Antennas Propag.*, Busan, South Korea, Oct. 2018, pp. 1–2, Paper WeG1-1.
[2] *Release 15 Description, V1.1.0.*, document 3GPP TR 21.915, Mar. 2019.
[3] *Active Antenna System (AAS) Base Station (BS) Transmission and Reception (Release 15)*, document V15.6.0 3GPP TS 37.105, Jun. 2019.
[4] H. Papadopoulos, C. Wang, O. Bursalioglu, X. Hou, and Y. Kishiyama, "Massive MIMO technologies and challenges towards 5G," *IEICE Trans. Commun.*, vol. E99-B, no. 3, pp. 602–621, Mar. 2015.
[5] J. Butler and R. Lowe, "Beam-forming matrix simplifies design of electronically scanned antennas," *Electron. Des.*, vol. 9, pp. 170–173, Apr. 1961.
[6] W. M. Dyab, A. A. Sakr, and K. Wu, "Dually-polarized Butler matrix for base stations with polarization diversity," *IEEE Trans. Microw. Theory Techn.*, vol. 66, no. 12, pp. 5543–5553, Dec. 2018.
[7] J.-W. Lian, Y.-L. Ban, J.-Q. Zhu, K. Kang, and Z. Nie, "Compact 2-D scanning multibeam array utilizing the SIW three-way couplers at 28 GHz," *IEEE Antennas Wireless Propag Lett.*, vol. 17, no. 10, pp. 1915–1919, Oct. 2018.
[8] A. Tajik, A. S. Alavijeh, and M. Fakharzadeh, "Asymmetrical 4×4 Butler matrix and its application for single layer 8×8 Butler matrix," *IEEE Trans. Antennas Propag.*, vol. 67, no. 8, pp. 5372–5379, Aug. 2019.
[9] K. Ding and A. A. Kishk, "Extension of Butler matrix number of beams based on reconfigurable couplers," *IEEE Trans. Antennas Propag.*, vol. 67, no. 6, pp. 3789–3796, Jun. 2019.
[10] S. Yamamoto, J. Hirokawa, and M. Ando, "A single-layer hollow-waveguide 8-way Butler matrix," *IEICE Trans. Electron.*, vol. E89-C, no. 7, pp. 1080–1088, Jul. 2006.
[11] C.-W. Wang, T.-G. Ma, and C.-F. Yang, "A new planar artificial transmission line and its applications to a miniaturized Butler matrix," *IEEE Trans. Microw. Theory Techn.*, vol. 55, no. 12, pp. 2792–2801, Dec. 2007.
[12] K. Ding and A. A. Kishk, "2-D Butler matrix and phase-shifter group," *IEEE Trans. Microw. Theory Techn.*, vol. 66, no. 12, pp. 5554–5562, Dec. 2018.
[13] M. Bona, L. Manholm, J. P. Starski, and B. Svensson, "Low-loss compact Butler matrix for a microstrip antenna," *IEEE Trans. Microw. Theory Techn.*, vol. 50, no. 9, pp. 2069–2075, Sep. 2002.
[14] A. A. M. Ali, N. J. G. Fonseca, F. Coccetti, and H. Aubert, "Design and implementation of two-layer compact wideband butler matrices in SIW technology for Ku-band applications," *IEEE Trans. Antennas Propag.*, vol. 59, no. 2, pp. 503–512, Feb. 2011.
[15] I. Stil, A. Fontana, B. Lefranc, A. Navarrini, P. Serres, and K. Schuster, "Loss of WR10 waveguide across 70-116 GHz," in *Proc. 22nd Int. Symp. Space THz Technol.*, 2012, pp. 1–3.
[16] R. A. Alhalabi and G. M. Rebeiz, "High-efficiency angled-dipole antennas for millimeter-wave phased array applications," *IEEE Trans. Antennas Propag.*, vol. 56, no. 10, pp. 3136–3142, Oct. 2008.
[17] R. Głogowski, J. Zürcher, C. Peixeiro, and J. R. Mosig, "Ka-band rectangular waveguide to suspended stripline transition," *IEEE Microw. Wireless Compon. Lett.*, vol. 23, no. 11, pp. 575–577, Nov. 2013.
[18] R. Glogowski, J.-F. Zurcher, C. Peixeiro, and J. R. Mosig, "Broadband Ka-band rectangular waveguide to substrate integrated waveguide transition," *Electron. Lett.*, vol. 49, no. 9, pp. 602–604, Apr. 2013.
[19] J. H. Acoraci, "Practical implementation of large Butler matrices," U.S. Patent 4 356 461 A, Oct. 26, 1982.
[20] Y. J. Cheng, W. Hong, and K. Wu, "A two-dimensional multibeam array antenna based on substrate integrated waveguide technology," in *Proc. Asia–Pacific Microw. Conf.*, Macau, China, Dec. 2008, pp. 1–4.
[21] Y. Li, J. Wang, and K.-M. Luk, "Millimeter-wave multibeam aperture-coupled magnetoelectric dipole array with planar substrate integrated beamforming network for 5G applications," *IEEE Trans. Antennas Propag.*, vol. 65, no. 12, pp. 6422–6431, Dec. 2017.

[22] J.-W. Lian, Y.-L. Ban, Q.-L. Yang, B. Fu, Z.-F. Yu, and L.-K. Sun, "Planar millimeter-wave 2-D beam-scanning multibeam array antenna fed by compact SIW beam-forming network," *IEEE Trans. Antennas Propag.*, vol. 66, no. 3, pp. 1299–1310, Mar. 2018.
[23] W.-Y. Chen, M.-H. Huang, P.-Y. Lyu, S.-F. Chang, and C.-C. Chang, "A 60-GHz CMOS 16-beam beamformer for two-dimensional array antennas," in *IEEE MTT-S Int. Microw. Symp. Dig.*, Tampa, FL, USA, Jun. 2014, pp. 1–3.
[24] T. K. G. Kwang and P. Gardner, "4×4 butler matrix beam forming network using novel reduced size branchline coupler," in *Proc. 31st Eur. Microw. Conf.*, London, U.K., 2001, pp. 1–4.
[25] S. Yamamoto, J. Hirokawa, and M. Ando, "A half-sized post-wall short-slot directional coupler with hollow rectangular holes in a dielectric substrate," *IEICE Trans. Electron.*, vol. E88-C, no. 7, pp. 1387–1394, Jul. 2005.
[26] T. Djerafi and K. Wu, "Super-compact substrate integrated waveguide cruciform directional coupler," *IEEE Microw. Wireless Compon. Lett.*, vol. 17, no. 11, pp. 757–759, Nov. 2007.
[27] T. Djerafi and K. Wu, "A low-cost wideband 77-GHz planar Butler matrix in SIW technology," *IEEE Trans. Antennas Propag.*, vol. 60, no. 10, pp. 4949–4954, Oct. 2012.
[28] J. A. Ruiz-Cruz, J. R. Montejo-Garai, and J. M. Rebollar, "Short-slot E- and H-plane waveguide couplers with an arbitrary power division ratio," *Int. J. Electron.*, vol. 98, no. 1, pp. 11–24, 2011.
[29] D.-H. Kim, J. Hirokawa, and M. Ando, "Design of waveguide short-slot 2-plane couplers for one-body 2-D beam-switching Butler matrix application," *IEEE Trans. Microw. Theory Techn.*, vol. 64, no. 3, pp. 776–784, Mar. 2016.
[30] D.-H. Kim, J. Hirokawa, and M. Ando, "One-body 2-D beam-switching Butler matrix with waveguide short-slot 2-plane couplers," *IEICE Trans. Electron.*, vol. E100-C, no. 10, pp. 884–892, Oct. 2017.
[31] D.-H. Kim, J. Hirokawa, and K. Nishimori, "Design of one-body 64×64-way 2-D beam-switching Butler matrix," in *Proc. IEEE Int. Symp. Antennas Propag.*, San Diego, CA, USA, Jul. 2017, Paper TUP-UB.3P.96.
[32] J. Hirokawa, D. Kim, M. Wakasa, Y. Sunaguchi, T. Tomura, and K. Nishimori, "Measurements of a 64×64-way one-body two-dimensional beam-switching hollow-waveguide Butler matrix," in *Proc. 48th Eur. Microw. Conf.*, Madrid, Spain, Sep. 2018, pp. 125–128.

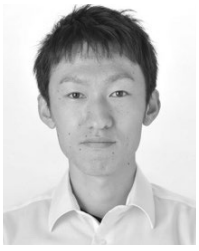

TAKASHI TOMURA (S'11–M'14) received the B.S., M.S., and D.E. degrees in electrical and electronic engineering from the Tokyo Institute of Technology, Tokyo, Japan, in 2008, 2011, and 2014, respectively.

He is a member of the IEICE. He was a Research Fellow of the Japan Society for the Promotion of Science (JSPS), in 2013. From 2014 to 2017, he was with Mitsubishi Electric Corporation, Tokyo, where he was involved in research and development of aperture antennas for satellite communications and radar systems. From 2017 to 2019, he was a Specially Appointed Assistant Professor with the Tokyo Institute of Technology, where he is currently an Assistant Professor. His research interests include electromagnetic analysis, aperture antennas, and planar waveguide slot array antennas. He received the Best Student Award from Ericsson, Japan, in 2012, and the IEEE AP-S Tokyo Chapter Young Engineer Award, in 2015, and the Young Researcher Award from the IEICE Technical Committee on Antennas and Propagation, in 2018.

DONG-HUN KIM (GS'09) received the B.S. degree in electrical and electronic engineering from Yonsei University, Seoul, South Korea, in 2008, the M.S. degree in environmental studies from Tohoku University, Sendai, Japan, in 2011, and the D.E. degree in electrical and electronic engineering from the Tokyo Institute of Technology, Tokyo, Japan, in 2017.

From 2011 to 2014, he was with the Materials & Components R&D Lab., LG Electronics, where he involved in the research of plasma diagnosis and the development of matching network for plasma lighting systems. Since 2017, he has been with SEMES Company, Ltd., Hwaseong, South Korea, where he is currently a Senior Engineer. His current research interests include microwave and RF in semiconductor equipment.

MASAHIRO WAKASA received the B.S. and M.S. degrees in electrical and electronic engineering from the Tokyo Institute of Technology, in 2015 and 2018, respectively. He joined JGC Corporation, in 2018, where he was involved in plant system designs.

YUKI SUNAGUCHI received the B.S. degree in electrical and electronic engineering from the Tokyo Institute of Technology, Tokyo, Japan, in 2018, where he is currently pursuing the M.S. degree.

JIRO HIROKAWA (S'89–M'90–SM'03–F'12) received the B.S., M.S., and D.E. degrees in electrical and electronic engineering from the Tokyo Institute of Technology (Tokyo Tech), Tokyo, Japan, in 1988, 1990, and 1994, respectively.

He was a Research Associate with Tokyo Tech, from 1990 to 1996, and an Associate Professor, from 1996 to 2015, where he is currently a Professor. He was with the Antenna Group, Chalmers University of Technology, Gothenburg, Sweden, as a Postdoctoral Fellow, from 1994 to 1995. His research area has been in slotted waveguide array antennas and millimeter-wave antennas. He received the IEEE AP-S Tokyo Chapter Young Engineer Award, in 1991, the Young Engineer Award from IEICE, in 1996, the Tokyo Tech Award for Challenging Research, in 2003, the Young Scientists' Prize from the Minister of Education, Cultures, Sports, Science and Technology in Japan, in 2005, the Best Paper Award, in 2007, and the Best Letter Award from the IEICE Communications Society, in 2009, and the IEICE Best Paper Award, in 2016 and 2018. He is a Fellow of the IEICE.

KENTARO NISHIMORI (M'99) received the B.E., M.E., and Ph.D. degrees in electrical and computer engineering from the Nagoya Institute of Technology, Nagoya, Japan, in 1994, 1996, and 2003, respectively. In 1996, he joined the NTT Wireless Systems Laboratories, Nippon Telegraph and Telephone Corporation, in Japan. He has been an Associate Professor with Niigata University, since 2009. He was a Visiting Researcher with Aalborg University, Aalborg, Denmark, from February 2006 to January 2007. He received the Young Engineers Award from the IEICE of Japan, in 2001, and the Young Engineer Award from the IEEE AP-S Japan Chapter, in 2001. He received the IEICE Best Paper Award, in 2010. His main interests include spatial signal processing including massive MIMO systems. He is a member of the IEICE.